Scalable Computing: Practice and Experience, ISSN 1895-1767, http://www.scpe.org
© 2024 SCPE. Volume 25, Issues 4, pp. 2687–2702, DOI 10.12694/scpe.v25i4.2826

TASK-DEPENDENT SLICING WITH CONVOLUTIONAL NETWORK MODEL FOR HISTOPATHOLOGICAL IMAGE ANALYSIS

N HARI BABU*AND VAMSIDHAR ENIREDDY†

Abstract. Due to its high rates of both mortality and morbidity, cancer stands as the primary cause of death globally. The examination of histopathological images plays a crucial role in the early prediction of cancer, relying on manual practices for each individual affected. However, this phase is prone to errors, time-consuming, and doesn't facilitate early-stage decision-making for pathologists. Despite significant advancements in computer-aided image processing, the analysis of histopathological morphology remains challenging due to the intricate nature of these images. Moreover, limited annotations restrict sample analysis. This work focuses on developing efficient deep-learning methods to analyze histopathological images by considering both global and local features. It involves the analysis of image patches and features to address issues related to image annotations. A unique task-specific slicing model, integrated with the convolutional network model (ts-CNN) is proposed. This framework aims to conduct patch-level feature examination and combine multiple samples to achieve the necessary outcomes for classification. The envisioned model aims to rectify inefficiencies present in various existing approaches. Using MATLAB 2020a, the proposed model was employed to classify cancer-based histopathological images, demonstrating superior predictive performance. It assisted pathologists in early cancer prediction with an accuracy of 98.2 % and aided in decision-making processes, offering promising results.

Key words: histopathological images, morphology, prediction, classification, and feature representation.

1. Introduction. Breast cancer (BC) is a highly prevalent form of cancer globally and is recognized as a significant contributor to mortality rates among women [1]. Histopathology images are the standard for diagnosing breast cancer [2]. Expert pathologists have previously employed powerful microscopes to examine tissue samples to diagnose tumours in cancer patients. Although this method is often used in clinical settings, it cannot be scaled up to clinical and translational research studies requiring many tissue specimens. It is a complex, time-consuming activity that requires expertise and is impacted by human characteristics like exhaustion and attention span. On the other hand, modern digital microscopy equipment can quickly take images of high-resolution tissue samples [3]. The implementation of computer-aided diagnosis (CAD) holds promise in enhancing tumour diagnosis and alleviating the workload of pathologists. BC histopathologic imaging analysis has drawn a lot of interest [4]. The automated differentiation of tumours into benign or malignant types utilizing sizable, openly accessible annotated datasets is the application of this technology that exhibits the most potential. Traditionally, relevant information from histopathology images has been extracted using techniques for feature extraction [5]. Several textural components that have been manually created, such as the Local Phase Quantization (LPQ), Grey-Level Co-Occurrence Matrix (GLCM), Local Binary Patterns (LBP), and Completed LBP (CLBP), have been utilized to distinguish between malignant and benign tumours. Jiang et al. [6] go into great detail about these characteristics. Sharma et al. [7] used Random Forest and Support Vector Machine (SVM), two well-liked classifiers to reach classification accuracy of 80 % to 85 %. Convolution neural networks (CNNs) have recently attained cutting-edge performance in image classification. Histopathology image processing in breast cancer research has employed classification methods that rely on data analysis. In their study, [8] employed the AlexNet deep learning model to distinguish between benign and malignant breast tumours based on pathology images. Compared to what was accomplished using a conventional machine learning algorithm, the categorization was 6 % better. With a recognition accuracy of 83

*Department of Computer Science and Engineering, Koneru Lakshmaiah Education Foundation, Guntur(D), Andhra Pradesh, India (harihod1@gmail.com)
†Department of Computer Science and Engineering, Koneru Lakshmaiah Education Foundation, Guntur(D), Andhra Pradesh, India (vamsidhar@kluniversity.in)

%, [9] classified breast pathology images without regard to magnification.

Shortly after, other papers recommended how CNNs could be enhanced for even greater accuracy. DeCAF characteristics, for instance, were employed by [10] to identify breast cancer with a 90 % accuracy rate. Breast cancer histopathology image categorization could be made more precise by utilizing the BiCNN model, which is a deep convolutional neural network, according to [11]. Up to 97 % classification accuracy was produced by this model. A multi-classification technique for identifying breast cancer was created and has a similar accuracy of 93.2 % on a vast dataset. Convolutional neural networks (CNNs) outperformed feature-based classifiers built up manually in a study by Zhu et al. [12]. For binary classification, the CNNs attained accuracy rates ranging from 96.15 % to 98.33 %, while for multi-class classification, they achieved rates between 83.31 % and 88.23 %. The MuDeRN framework, developed by Mozejko et al. [13], has demonstrated high accuracy in classifying breast histopathology images, achieving correct classification rates of up to 98.52 % in binary classification. Additionally, convolutional neural networks (CNNs) have been successfully employed in various tasks, including identifying breast cancer mitosis and detecting metastases [14].

Deep learning has made remarkable advancements in image recognition; however, its implementation in the medical sector is limited due to its dependence on large-scale training datasets. Guo et al. [15] have highlighted the lack of substantial, annotated, and publicly available datasets as a significant obstacle to advancing novel histopathological image analysis tools. There has yet to be much research that aims to alleviate the load of annotating. Our earlier study [15] aimed to reduce the annotation required for histopathology image classification by applying deep domain adaptation to extract strong, domain-specific characteristics. As a result, a classification model of this type that was trained on a source domain with all labels present can be applied immediately to a target domain. The classification performance was still constrained for clinical applications, and an entirely supplementary dataset was necessary [15]. The suggested approach uses active learning, which doesn't need an additional dataset, to reduce complex manual labelling.

In this study, we anticipate a deep learning system to reduce expenses related to annotation for classifying breast cancer histopathology images. Our approach will assist pathologists in labelling data. The model is initially given a minimal dataset, which it proactively learns by choosing the unlabeled data to be categorized through a learning approach. The actively selected examples are used to refine this deep model gradually. The proposed task-dependent slicing model is integrated with the convolutional network model (ts-CNN) and operates two distinct techniques. The first method updates the model by picking samples for labelling those with the highest level features based on the provided examples. This approach to inquiry is frequently used in active learning and is regarded as a best practice. The classification strategy aims to enhance confidence by concurrently considering samples exhibiting high confidence and feature mapping. The idea indicates that new supervision should be included in addition to the categorization model's current rules. This study examines the effectiveness of slicing-based methods for BC histopathology image collections. We then analyze and draw conclusions based on comparing these different approaches. Our findings indicate that the slicing strategy can significantly reduce annotation costs for binary classification of BC histopathology images, achieving a reduction of up to 67 %. Similarly, the slicing-based technique demonstrates a potential decrease in annotation costs by up to 60 %. The proposed model helps the physicians to take decision during tough times and act as a Clinical Decision Support System (CDSS). It functions as the human machine interface system to deal with the emergency situation to treat the patients.

The work is drafted as follows: section 2 provides a broader analysis of diverse approaches. The methodology is elaborated in section 3. The numerical outcomes are provided in section 4, and the work is summarized in section 5.

2. Related works. The prognosis is improved, and the patient survival rate is increased to 50 % due to early and precise identification. Correctly classifying each cancer stage is necessary to diagnose BrC [16]. In contrast to previous BrC testing methods, different medical imaging is frequently employed to analyze BrC effectively [17]. Breast cancer (BrC) is commonly detected through various medical imaging techniques such as sonograms, MRIs, histopathology images, mammography, and magnetic resonance imaging (MRI). For a precise BrC diagnosis, a pathologist's expertise and topic knowledge are needed. Without them, misdiagnosis happens frequently, especially when BrC is still in its early phases [17]. The early detection of BrC is vital, though. A lot of computer-aided diagnosis (CAD) tools are employed by doctors to help them detect breast cancer early

on in mammograms. It is a simple approach for early BrC diagnosis that is quick, dependable, and economical [19]. The accuracy of BrC identification has increased by more than 20 % thanks to CAD developments during the past ten years. The mortality rate is reduced from 30 % to 70 % thanks to this method, which aids doctors and radiologists in identifying anomalies utilizing various imaging modalities [20].

By merging data from several domains, including pathology, radiology, pharmacology, cardiology, genomics, and cancer, deep learning (DL) based CAD systems have exhibited substantial breakthroughs [20] in the medical field. For the diagnosis and prognosis of illnesses, including cancer, DL has become a well-known machine learning-based technique. Since machine learning-based technologies for cancer detection have been continuously improving in recent years, it has become clear that DL is adequate in both cancer prognosis and prediction [20]. Deep learning (DL) has demonstrated superior diagnostic accuracy in breast cancer imaging compared to mammograms, ultrasounds, and digital breast tomosynthesis (DBT). This increased accuracy has led to the adoption of DL in clinical breast cancer (BrC) treatment [21]. Numerous studies on using deep learning in BrC have been published recently. These studies highlight the effectiveness of deep-learning algorithms in addressing the challenges and intricacies associated with automated BrC diagnosis. BrC classification has been the subject of numerous review studies, but few of them have been able to offer unambiguous guidance for future researchers [22]. Although these papers provided an excellent literature review on BrC, they could have covered more topics related to deep learning. The existing literature on BrC has predominantly concentrated on traditional machine learning (ML) methods and generic artificial neural networks (ANNs), with an emphasis on feature extraction for diagnostic purposes [23]. However, more attention should be given to newer deep learning architectures such as extreme learning machines (ELMs) and generative adversarial networks (GANs) in the context of BrC diagnostics. Additionally, previous review papers have yet to comprehensively evaluate the strengths and weaknesses of earlier studies [24], resulting in a lack of clarity in their analysis of deep learning-based techniques. This paper presents a comprehensive examination of recent advancements in the categorization of breast cancer (BrC) images through the utilization of deep learning in computer-aided diagnosis (CAD) [25]. The analysis encompasses six distinct perspectives: the model architecture employed for diagnosis, the datasets utilized, image pre-processing techniques, the strategy employed for breast cancer imaging, the metrics employed for evaluating performance, and potential avenues for future research. These perspectives are used to address the study's limitations [26].

The goal values are adjusted using back-propagation, an unsupervised learning technique, via auto-encoder. The input, decoding, and hidden layers are the three layers that make up a neural network. Using an auto-encoder, the input is transformed into the hidden layer. The decoder then reconstructs the input from hidden layer's starting point. There are four main kinds of auto-encoders: the contractive auto-encoder (CAE), the variational AE, the sparse AE and the denoising AE [27]. A denoising version of the stacked auto-encoder is the stacked denoising AE. Using AE, we benefit from data's reduced dimensionality. Hyper-parameter tuning, processing time, data and model validation are all required for auto=encoder training. Although auto-encoder and principle component analyses (PCA) are relatively similar, PCA is less versatile than an auto-encoder. An auto-encoder can carry out both linear and non-linear transformations, whereas PCA is limited to performing solely linear transformations [28].

Given the significance of the convolutional neural network (CNN) in classifying breast cancer, it is imperative to examine this computational model comprehensively. In earlier works, CNNs were more frequently used to create a reliable cancer classification model. CNNs function well with images and are used with several imaging modalities. To train a CNN, however, a lot of images are required. With a small number of images, good performance is challenging to accomplish. Furthermore, because labelled datasets in medical imaging are expensive to generate, finding appropriate training data is difficult. CNN, however, has a lot of benefits. A ConvNet needs substantially less pre-processing than other classification techniques. A single CNN architecture combines feature extraction and classification as a whole. Finally, it is immune to local geometric distortions and visual noise. To facilitate the extraction of essential features from medical images and subsequently conduct breast cancer classification, researchers have employed convolutional neural networks (CNNs) [28]. Histolopathologic image analysis plays a pivotal role in cancer diagnosis, wherein histopathologists visually scrutinize cell shapes and tissue distributions to assess irregularities. Their evaluation involves determining whether specific tissue regions exhibit signs of cancer and gauging the degree of malignancy present in these areas. The proposed

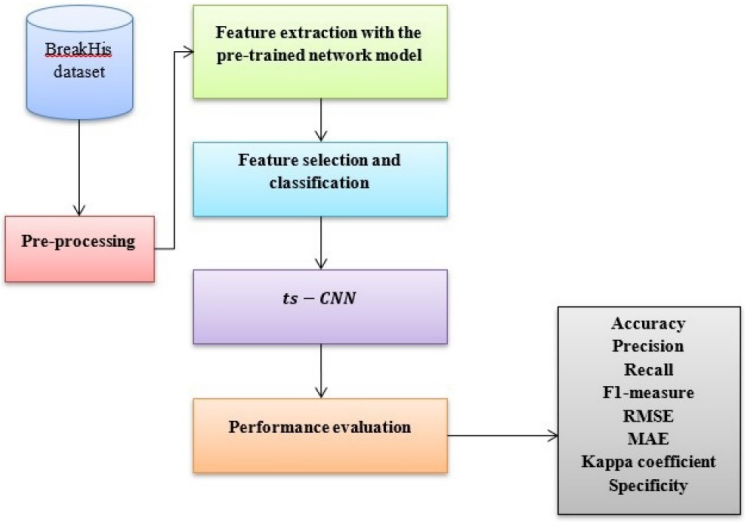

Fig. 3.1: Block diagram

model helps in predicting the cancer using CDSS, i.e. human machine interface system effectively.

3. Methodology. Fig 3.1 depicts the block of the anticipated model where the samples are taken BreakHis dataset where pre-processing performed to normalize the samples. The features are extracted and fed to the classifier (ts-CNN) where the performance is evaluated with various metrics like accuracy, precision, recall and so on. The convolutional network model (ts-CNN) is merged with the task-dependent slicing model. This study describes a technique for categorizing histological images of breast cancer employing only global labels. In this approach, transfer learning trains a pre-existing network to extract patch features. The novelty of the proposed model is its efficiency to access the classification accuracy using the task-based slicing model. The convolutional network is designed to differentiate the cancer images based on the class labels. The proposed model establishes better testing outcomes from the slicing model. It is more significant as the proposed model has to differentiate the image malignancy and benign regions to offer better medical prediction. Owing to the constraint accessibility of labelled histological breast cancer images, it is necessary to perform task-slicing. The image-level labels used to label the datasets allow for the application of MIL to choose the discriminative patch features. A combination of positive and negative examples is selected to generate an image-level feature. As seen in Fig 3.1, the proposed approach is broken down into four key elements. The necessary feature at the patch level was extracted in the first step. These patch-level features are combined to describe the image-level feature comprehensively. The final whole slide image (WSI) feature is created by selecting the discriminative characteristics at the end. Finally, abnormal and standard images of breast cancer histology are distinguished. Here, a breast histological image with tumours or cancer is used to signify an aberrant histopathological image.

3.1. Feature extraction with ResNet50. Even though a CNN is capable of classifying images on its own, it is unfeasible to use CNN to identify histopathology images with more than 100,000*100,000 pixels directly. The histopathology images, however, will lose too much information if they are resized to fit on a CNN. Given these considerations, the histological image of breast cancer is divided into smaller sections, referred to as patches, and subsequently magnified to a resolution of (224* 224) pixels. Additionally, patches with a background area percentage of more than 50 % are eliminated. The complex features of breast cancer histology images are difficult for both shallow and deep networks to handle. The complex clinical variables found in breast cancer histopathology images cannot be learned or matched by a deep neural network. We have chosen to use ResNet, a neural network architecture that facilitates training and generates good results. This is due to the lack of training data in histology and the benefits of residual learning through shortcut connections.

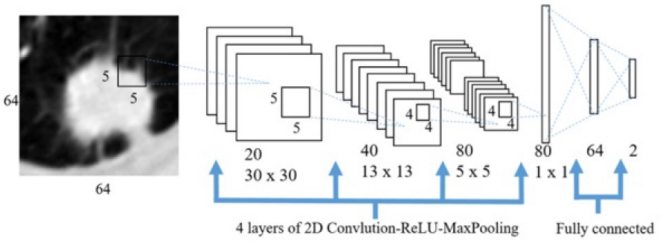

Fig. 3.2: Task-independent slicing CNN

ResNet-50 is used to process every patch taken from a whole histopathological image of breast cancer. The ResNet-50 model is initially trained using ImageNet dataset consists of 3.2 million high-resolution images. The last convolution layer provides the attributes of the patches. These attributes, referred to as P, are consistently represented as 2048*1 matrix. The fixed size of the input patches in the CNN which are always (224*224) pixels.

Aggregating local features extracted from patch-level feature vectors generates an image-level feature vector. This approach has been found to enhance the accuracy of classifying breast cancer histopathology images when relying solely on global labels. Max pooling, p-norm pooling, mean pooling and other popular methods can all be used to conduct local feature aggregation. Selecting the maximum pixel value within patch as representative value for feature aggregation is commonly called "max pooling" in the context of feature aggregation. In contrast, mean pooling calculates the aggregated feature value by determining the average pixel value within a patch. On the other hand, P-norm pooling retains valuable information from the patches while condensing the signal obtained from multiple patches. P-norm pooling was used in this experiment to identify the aggregated feature vectors. The following is an example of an aggregated feature:

$$f_p(v) = (\frac{1}{N}\sum_{i=1}^{N} v_j^p)^{\frac{1}{N}} \tag{3.1}$$

The present investigation also employed the feature vector of the i^th patch, represented as v_i^p and the overall count of patches in the histopathological image denoted as N. Here, P=3 was used in the investigation, specifically 3-norm pooling.

4. Feature selection. This study obtained image-level feature descriptors using the multiple features learning technique, which resembles previous works. This technique was used to extract more discriminative features while minimizing the presence of redundant or irrelevant features for classification. Instead of using image-level features readily derived from patch-level features, limited set of meticulously chosen and representative characteristics were employed to classify breast cancer pathology images. Histological images of breast cancer can be quickly and inexpensively described. The selected characteristic is derived from the combined features rather than the labels assigned to the patches to differentiate between the affected and healthy breast tissue sections. Here, the histological image of the breast tissue is viewed as a bag containing numerous examples, particularly the patches that have been removed from it. A patch is considered a negative instance of breast cancer detection if it has no breast cancer tissue. A patch incorporating breast malignant tissue, on the other hand, is thought to be a positive instance. At least one positive occurrence in a histopathological picture indicates an abnormal condition, while the absence of any positive instances suggests a normal state. Using this approach, we selected specific features from the instances and arranged them to derive the image-level feature. It was established how many top or bottom aspects of the cases were chosen as K. Since the available breast histological training images for breast cancer histopathology comprise typical regions and complex clinical features, the final features were selected by choosing the top and bottom K pixels. The histopathological image's feature vector, designated as $f_p(v)$, was initially sorted according to the pixels. The sorted vector is presented

in the following written form:

$$f_{sort} = (v_1^{'}, v_2^{'}, ..., v_p^{'}) \tag{4.1}$$

In this method, the dimensions of the vector f_p^v are represented by P = 2048. The image-level vector f_{diff} is created by combining top-K and bottom-K pixels of the sorted f as stated in Eq. (4.1). This approach effectively utilizes both the top regions, which indicate positive cases related to cancer and bottom regions which show negative instances related to cancer.

5. Classification using ts-CNN. In breast histopathology image classification, image-level features are obtained through a series of steps, including selection, feature extraction, and patch extraction. By selecting K highest and lowest pixels from sorted vectors where the input feature vectors for classifier are generated. These vectors are then transformed into image-level characteristics with dimensions of 2*K, as illustrated in Fig 3.2. In our study, we employed a multilayer perceptron as the ultimate classifier to investigate the interplay between the upper and lower pixel values more comprehensively, despite the satisfactory performance of a standalone CNN classifier. Fig 3.2 shows the multilayer perceptron's architectural layout. Our research used a multilayer perceptron with two ultimately linked layers and 200 and 100 neurons each. ReLU was used as the activation function. A two-neuron output layer was used to determine if the input breast histopathological images were normal or abnormal to binary classify breast cancer histological images.

6. Network training. In our experiments, we used substantial regularization and data augmentation to avoid over-fitting caused by insufficient training photos. In the initial layers of the multilayer perceptron, we applied L2-regularization and dropout at rates of 0.5. The suggested architecture runs more effectively with the default Adam optimizer despite recent improvements in optimizers to increase the effectiveness of deep networks. In this study, the Adam optimizer was employed to minimize the binary cross-entropy loss, utilizing a batch size 24 and a learning rate of 0.001. The classification model was developed using the MATLAB 2020a framework, which is an open-source platform. A learning model was constructed to enhance the accuracy of classifying breast histopathology image data, each with distinct weights. The projected outcome for a histology image was determined by averaging predictions generated by E models with E set to 10. The proposed ts-CNN is trained in 70 % samples where the prediction accuracy with these samples are higher, i.e. 98.2 % where the testing is done with remaining 30 % samples. The training process consumes 1000s which is optimal compared to other approaches.

7. Numerical results and discussion.

7.1. Dataset acquisition. BreaKHis, a sizable, publicly accessible, and annotated dataset that includes histopathology images of breast cancer (BC), was used to evaluate the proposed system. This dataset encompasses 7,909 microscopic images, including 24 images of benign tissue and 58 images of malignant tissue. The P & D laboratory in Brazil collected images from 82 patients. Each patient has many histopathological images collected and given the same labels as the patients. Breast tissue biopsy slides that have undergone a conventional fixation, dehydration, embedding, and trimming technique are used to create image samples. Hematoxylin and eosin (H & E) staining introduces colour to the slides. In particular, (40X,100X,200X,and 400X) are prominent magnifications used to capture many of the images in the collection. These magnifications are equivalent to the corresponding objective lens magnifications of 4X,10X,20X,and 40X. The four magnifications' respective effective pixel sizes are 0.49µm, 0.2µm, 0.1µm, and 0.05µm. 2,480 normal images and 5,429 malignant ones are included in the collection. Each image has been encoded using three channel RGB format with 8bit depth for every channel and measures 700 by 460 pixels in size. The PNG file format is used to store all images. The images are labelled by pathologists with labels like benign and malignant.

7.2. Execution. The MATLAB 2020a framework is used to put the suggested method into practice. The ts-CNN architecture is the foundation of the deep model; a pre-trained network was trained on the provided dataset. The server has an NVIDIA GeForce GTX 1080Ti GPU and Intel 3.6 GHz CPU. BreaKHis dataset is divided into two different sets: a testing set called B _test and a training sample pool called B _pool. These sets do not overlap. Before training, it is ensured that the malignant and benign samples in the Btest are balanced. Then, B _pool receives the remaining samples. Rotational and symmetric data augmentation

Table 7.1: Statistical distribution

Factors	Benign	Malignant	Total
4X	625	1370	1995
100X	644	1437	2081
200X	623	1390	2013
400X	588	1232	1820
Samples	024	0058	0082

techniques are employed in the training samples to balance imbalance malignant and benign samples in B _pool. The parameters for B _pool and B _test are the same as in [30], with B _pool/B _test remaining at 70 %/30 %. Table 7.1 displays the distribution of augmented datasets. The task-dependent slicing model with the convolutional network model (ts-CNN) architecture was selected for our research due to its advantageous combination of network depth and convergence speed. Before inputting the images into the neural network, they are resized to a dimension of 227*227 pixels. The convolutional neural network's W parameters are updated using the Adam optimizer. When the network is trained, the learning rate is 105. The average of five experiments produced the findings provided in this study. The parameters W are estimated using the samples and matching labels (training set) in data-driven methods known as ts-CNN. The parameters are then utilized to categorize testing data after training. The parameters are adjusted even more precisely if more data is generated.

7.3. Metrics. The suggested methods are assessed on a pair of levels. An image is initially classified as "benign" or "malignant" using a binary classification technique at image level. The classification accuracy serves as validation measure because the distribution of categories at the image level is balanced. According to this definition, this accuracy:

$$Accuracy = \frac{N_c}{N_{im}}(image - level) \tag{7.1}$$

When classifying images, the variables N_c and N_{im} represent the total classified images (correctly) and total images (dataset), respectively.

Subsequently, patient-level classification, evaluates the precision of recognizing images for each distinct patient. The factors N_p, N_{im}^p and N_c^p govern this assessment. The three numbers N_p, N_{im}^p and N_c^p represent the total count of pictures successfully categorized for patients p. N_p indicates the overall number of patients.

$$Accuracy = \frac{\sum_{i=1}^{N_p} \frac{N_c^p}{N_{im}^p}}{N_p}(Patient \quad level) \tag{7.2}$$

The parameter selection approach's efficacy was assessed by examining its classification performance on the validation dataset. Breast cancer histological image categorization was done on dataset to measure method's accuracy. The accuracy was assessed by contrasting the actual and expected breast histopathology images. To evaluate the effectiveness of the method's categorization, several performance metrics like true negatives (TN), false negatives (FN), true positives (TP), and false positives (FP), were calculated. By calculating the percentage of accurately predicted abnormal breast histopathological images among all of the predicted abnormal breast histological images, the model's accuracy was also measured. The recall, or actual positive rate, was calculated by partitioning number of precisely predicted abnormal breast histology images by total abnormal breast histological images. The receiver operating characteristic (ROC) curve was utilized (See Fig 7.8) as evaluation metric when breast histology images changed. ROC curve is commonly recommended for evaluating results obtained through medical image processing. Additionally, using MATLAB 2020a, the F1-score, which ranges from 0 to 1, was calculated for the binary categorization of breast cancer histology images. Instead of preferring one over the other, the assessment tool used in this study is made to give equal weight to both precision and recall. The F1-score is more sensitive to unbalanced data than the Area under the

ROC curve (AUC). Eq. (7.3) to Eq. (7.9) are used to calculate the F1-score, recall, precision, and accuracy, respectively [15].

$$recall = \frac{TP}{TP + FN} \tag{7.3}$$

$$precision = \frac{TP + TN}{TP + FP} \tag{7.4}$$

$$precision = \frac{TP + TN}{TP + TN + FP + FN} \tag{7.5}$$

$$F1 - score = \frac{2 * precision * recall}{precision + recall} \tag{7.6}$$

$$K = \frac{P_{observed} - P_{chance}}{1 - P_{chance}} \tag{7.7}$$

$$MSE = \frac{1}{m}\sum_{i=1}^{m}(x_i - \hat{x_i})^2 \tag{7.8}$$

$$RMSE = (\sqrt{\sum_{i=1}^{m}\frac{1}{m}(\hat{x_i} - x_i)^2} \tag{7.9}$$

7.4. Validation. This study utilizes breast histopathology images for categorization. The authors used transfer learning to extract patch characteristics from the images, and multiple-feature learning was used to provide image-level features. The decision of positive and negative examples directly affects the image-level feature, affecting the classification results. A validation dataset comprising 70 breast histopathology images was used to assess the impact of various K values on categorization. According to the findings, accuracy and the F1-score initially rise and subsequently fall as the K value increases from 5 to 200. When K is set to 10, the suggested technique achieves an F1-score of 0.86 and an accuracy of 0.86. Notably, the approach operates best with K equal to 100, producing an F1-score of 0.99 and an accuracy of 0.986. Compared to the results obtained when K is set to 10, these values show 13 % and 12.6 % improvements, respectively. When K is increased to 200, there is 26 % and 17.4 % reduction in the F1-score and accuracy of the classification findings, respectively (See Fig 7.6). These results imply that the image-level feature vector, comprising the top 100 and bottom 100 pixels of the aggregated features, best represents the histopathological image's characteristics (See Fig. 7.1 and 7.5). Table 7.1 to Table 7.4 shows the experimental outcomes of the anticipated model. The advantage of the proposed model over the existing research is its efficiency to access the classification accuracy using the task-based slicing model. The convolutional network is designed to differentiate the cancer images based on the class labels which are generally a complex task encountered by the existing approaches. The proposed model establishes better testing outcomes from the slicing model. It is more significant as the proposed model has to differentiate the image malignancy and benign regions to offer better medical prediction. Therefore, the anticipated models' performance is compared and evaluated for accuracy and performance with other approaches to project its significances.

Detailed representations of the previously mentioned results are shown in sub-images to highlight how varying values of K lead to various categorization outcomes. For K values of 10, 100, and 200, the ROC curves in Fig 7.8 show considerable changes in the classification outcomes. Our tested method consistently generates classification scores above 0.85 when only a limited number of top and bottom pixels are extracted from the

Table 7.2: Comparison of annotation cost

Accuracy (%)	**Image State (%)**	**40X**	**40X**	**100X**	**100X**	**200X**	**200X**	**400X**	**400X**
Image level	Active	Acc	AC	Acc	AC	Acc	AC	Acc	AC
Image level	Std	89	400	91	250	92	450	90	350
Image level	Active	88	400	91.7	300	91	550	89	500
Image level	Pre-trained	87	700	91	750	91	750	90	750
Patient level	Std	91	350	93	300	93	400	92	350
Patient level	Active	90	400	92	400	92	400	92	450
Patient level	Pre-trained	91	700	92	750	93	750	92	600

Table 7.3: P-value computation

p-value	**Magnification**	**Magnification**	**Magnification**	**Magnification**
P-Value	00040X	00100X	0200X	00400X
Image-level based	00.017	00.003	0.003	0.0014
Patient-level based	0.0012	0.0001	0.005	0.0008

aggregated feature vector, such as K=10. The classification performance declines with a more significant K number, such as K=200, with an accuracy of 0.819, recall of 0.83, and precision of 0.69. The complexity of clinical characteristics and the size of histological images of breast tissue account for the changes brought on by K values. The final output's image-level feature displays various features in both standard and diseased breast tissue based on the selected K values. Identifying abnormal tissue characteristics is only partially attainable when the K value is low. On the other hand, if the K value is too high, too many features associated with normal tissue may be present in the image-level attributes of diseased tissues. Consequently, selecting the appropriate K value is crucial for correctly classifying breast cancer histology images using only global labels. For the following discussion, where we assess the classification performance on the testing dataset, we selected a K value of 100, considering both the classification performance and the network's training expenses.

8. Experimental outcomes. All images above were subjected to pre-processing before being utilized as input for the model. Based on the resulting output, the convolution layers' parameters were established during the training phase. Furthermore, these parameters remained unchanged during the validation process but were tested against the model using a test image to determine their accuracy and potential need for adjustment. The maximum average accuracy achieved through this approach over 100 epochs was 97.49 %. Weighted accuracy, which refers to the average true positive rate attained for each class, was used to adjust for the unbalanced dataset. Fig 7.6 displays the variations in accuracy between the test and train datasets during training. The results for $\lambda = 0.02$ are shown. The ROC curve is a crucial tool for evaluating the classifier's performance on the test dataset. This graph compares the sensitivity (rate of true positives) and specificity (% of false positives) for various threshold values of the parameter. Each point on the ROC plot represents a mix of false-positive and true-positive rate values for a particular threshold. In this scenario, the malignancy of benign tumours, the Area Under the Curve (AUC), shows how effectively the classifier can distinguish between diseased and normal classes. The task-dependent slicing model is integrated with the convolutional network model (ts-CNN), as seen in Fig 7.8 ROC curve. The TPR and FPR of the anticipated model is provided in Fig 7.8 where the positive predictions are higher compared to false positive. This shows the efficiency of the proposed model. Our suggested model distinguished between benign and malignant lesions with a valid AUC of 98.3 %. To evaluate its performance in differentiating between various sub-classes of lesions, as classified by Boman and Volminger. This work applied our suggested approach to comparable lesion images. The proposed model's computational specifications are listed below.

ROC curves illustrating the ts-CNN performance are shown in Fig 7.8. The ts-CNN model, trained to incorporate a novel regularizer, is evaluated on varying numbers of images for each case. Specifically, Fig 7.8 showcases the ROC curve from analyzing 33 melanoma images and 97 nevi images. Fig 7.8 illustrates the

Table 7.4: Performance Metrics Comparison

Metrics	ts-CNN	nl-SVM	IC-CSO	CNN	BiLSTM	DNN	CapsNet
Accuracy	98.2	97.5	95.7	94.3	94.8	91.8	93.4
Precision	98.5	97.2	95.6	94.5	94.5	90.5	92.2
F1-measure	98.3	97.4	95.5	93.7	92.2	90.4	91.9
Recall	98.1	97.2	95.5	94.9	0093	0091	91.6
Kappa	97.5	96.9	95.2	91.5	90.5	0081	83.7
Specificity	98.6	97.5	95.1	93.9	94.5	0091	91.6

Table 7.5: Error Metrics Comparison

Metrics	ts-CNN	nl-SVM	IC-CSO	CNN	BiLSTM	DNN	CapsNet
MAP	00.032	00.045	00.055	0.1915	0.201	0.286	0.2635
MAE	0.0019	0.0025	0.0030	0.0365	0.042	0.082	0.0696
RMSE	0.0021	0.0026	0.0032	00.035	0.043	0.083	00.070

ROC curve from examining 65 basal and squamous cell carcinoma images and 70 seborrheic keratosis images. The ROC curve resulting from the evaluation of 33 melanoma images and 97 seborrheic keratosis images is displayed in Fig 7.8. Lastly, it exhibits the ROC curve from analyzing 20 melanoma and 20 solar lentigo images. The AUC for each test in the above cases is shown in Table 7.1. Regarding the Area under the receiver operating characteristic curve (AUC-ROC), our ts-CNN with a unique regularizer outperformed the presented technique. We discovered that the AUC-ROC of nevus was 6.5 % higher than melanoma's. The AUC-ROC increased by 1.6 % in seborrheic keratosis, much like basal and squamous cell carcinoma. Our classifier compared seborrheic keratosis and melanoma well, increasing AUC-ROC by 1.13 %. AUC-ROC for classifying melanoma against solar lentigo was also achieved, and it was 86.35 %, outperforming prior values reported by 3.35 %. This research study hypothesized that using ts-CNN would result in more accurate categorization of binary comparisons between seborrheic keratosis and basal and squamous cell carcinoma, and nevus and melanoma, compared to other techniques. According to [25], three-way classification accuracy with a standard deviation of 0.9 % was 72.1 %. According to [28], the maximum accuracy ever found in literature is 93.64 %. However, our suggested method outperformed these figures published by previous authors, with a maximum average accuracy of 97.49 %. Although we experimented with various regularizer values, including $\lambda 0.2, 0.02, and 0.002$, the accuracy that produced the best results was $\lambda 0.02$ with a precision of 97.49 %. Table 7.3 contrasts our work with many other methodologies. The proposed model outperforms the current models, according to our findings. Due to the intricate variations in the appearance of histopathologic images, automated classification through images poses a significant challenge. To tackle this and achieve precise differentiation among the minutely detailed object categories, the proposed ts-CNN model have been employed. This study introduces a novel prediction model designed to classify images as either benign or malignant using a unique slicing technique. It serves as a binary classifier, distinguishing between these two categories of images. The proposed model demonstrated an impressive average accuracy of 98.2 %, showcasing its superiority over current state-of-the-art methods. The ts-CNN performance, measured in terms of ROC with the integrated novel task-slicing technique, was evaluated across various scenarios. The AUC achieved for differentiating nevus from melanoma lesions, seborrheic keratosis from basal cell carcinoma lesions, seborrheic keratosis from melanoma lesions, and solar lentigo from melanoma lesions respectively. These outcomes indicate that our proposed learning model surpasses existing algorithms and can serve as a valuable tool to aid medical practitioners in accurately classifying diverse types of cancer.

Malignant cells found in breast tissue are used to diagnose breast cancer, which affects one in eight women worldwide. Using a variety of methods, histopathology images captured under a microscope are the foundation of modern medical image processing. These days, processing pathological tools and medical images requires machine learning. Cancer cell detection by hand is time-consuming and prone to human mistake. As a result,

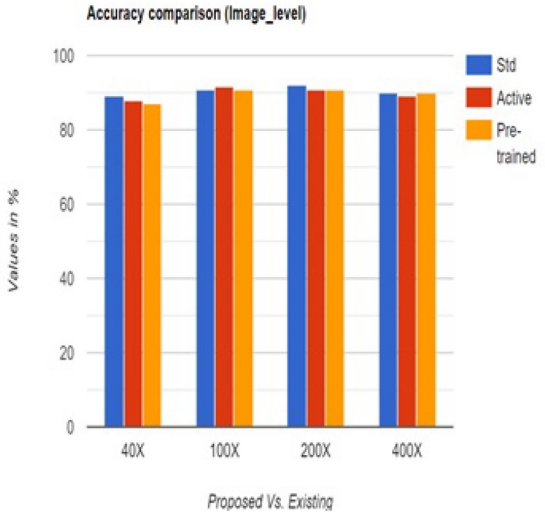

Fig. 7.1: Accuracy comparison (Image level)

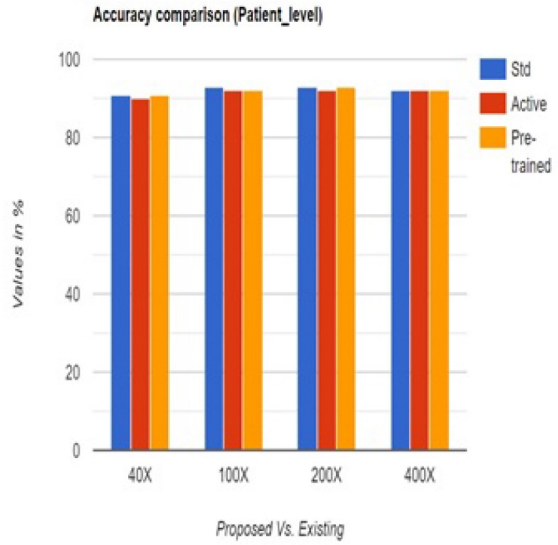

Fig. 7.2: Accuracy comparison (Patient level)

compared to manual systems, computer-aided mechanisms are used to get more accurate results. Medical imaging is a field that heavily utilizes deep learning, particularly via CNNs. With this method, features are extracted using CNN and then classified through a fully connected network. Its use in the medical industry is beneficial because it doesn't require any prior knowledge in the discipline. We trained a convolutional neural network in this study, and the result was an amazing prediction accuracy of up to 94.6 %. In this work, a CNN model called HIC-net is presented. Its purpose is to automatically identify malignant spots in whole-slide histopathological images (WSI). HIC-net's innovative architecture divides the WSI into distinct planes in order to use window-based classification. Our method includes an efficient WSI pre-processing step to improve predictability and speed up training.

Researchers can learn a great deal about cancer from the examination of histopathological images, but

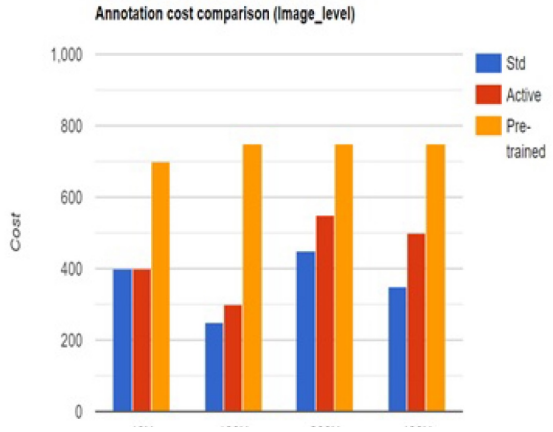

Fig. 7.3: Annotation cost comparison (Image level)

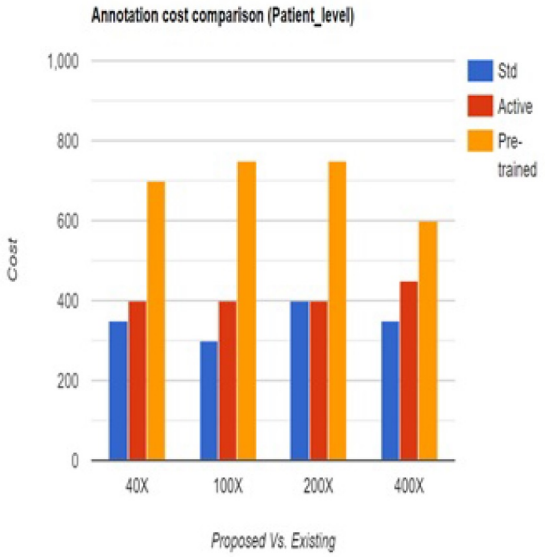

Fig. 7.4: Annotation cost comparison (Patient level)

the inherent difficulties with these images frequently make the analysis process take longer. In this work, a strong solution to the problem of classifying histopathology images is presented. To counteract the impact of background disrupting variables and reduce the complexity of histopathology pictures, a unique pre-processing procedure has been used. Both pathologists and machine learning algorithms face major problems when it comes to the analysis of histological images. Pathologists frequently dedicate hours to examining a single whole-slide tissue sample. Even if machine learning algorithms provide results more quickly, many of them have difficulty performing at the required level. This is frequently ascribed to the high image quality and the existence of distracting elements.

This work adopts a unique strategy in comparison to the literature currently in publication, where CNN architecture has shown impressive success and quickness in classification when compared to other methods. Rather of using a generic CNN architecture, a specific architecture that is specifically designed to fit the texture of histopathology images has been created. First layer of CNN architecture is a special preprocessing step based

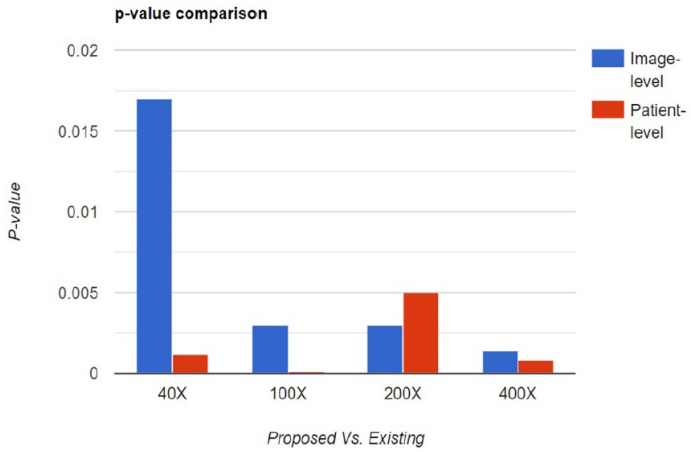

Fig. 7.5: P-value comparison

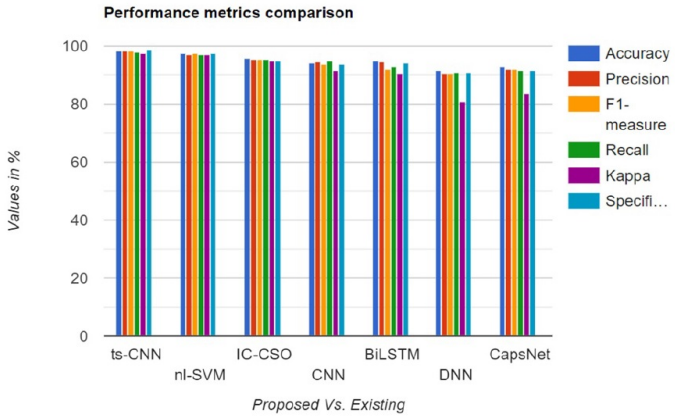

Fig. 7.6: Performance metrics comparison

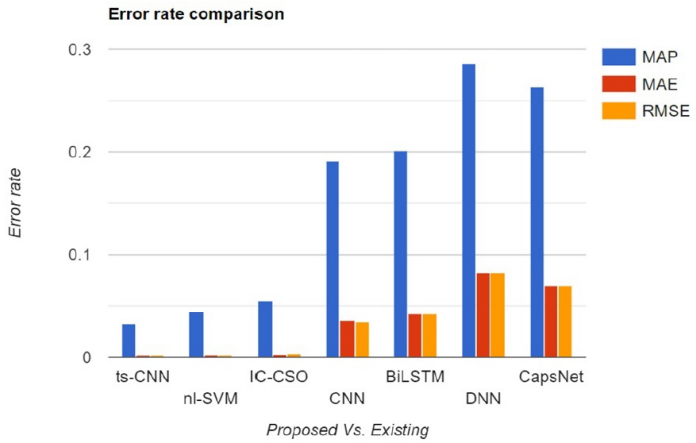

Fig. 7.7: Error rate comparison

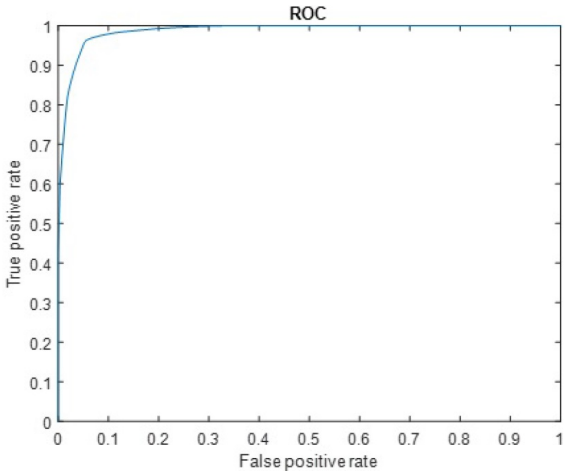

Fig. 7.8: ROC comparison

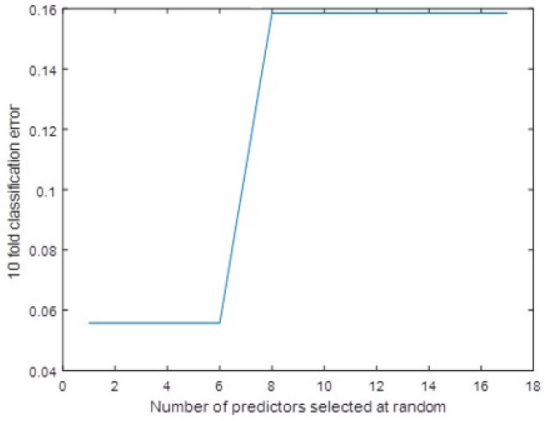

FIG. 7.9. *Classification error*

Fig. 7.9: Classification error

on the effect of H & E stained components and cell behavior. First, the high-resolution histopathology pictures should be normalized. Then, they should be segmented into smaller pieces in a particular order. Before being supplied into the network as the CNN input, every image fragment is subjected to the suggested medical image preprocessing procedure.

Due to its perceived lack of transparency in decision-making, deep learning is often criticized and labeled as a "black box." Even if it's known that humans don't always make perfect "white box" selections, there is always a desire to know why decisions are made. It's possible that this curiosity will spark fresh research in the subject of pathology. Although obtaining total transparency is still a difficulty, various research projects have looked for answers. One method to solve this problem has been investigated: collaborative learning that integrates diagnostic information and diseased visuals with attention mechanisms. An increasing number of people are interested in analyzing digital histopathology pictures because of the expanding repository, especially in the field of computer-aided diagnosis using machine learning techniques. Digital pathological pictures and related tasks provide special obstacles despite the possible advantages. We explore the use of machine learning techniques in the examination of digitally diseased photos in this mini-review. We also point out particular

problems that come with this kind of study and suggest possible fixes.

9. Constraints. Different investigators employ various regularization techniques. Regularization procedures that are frequently used include lasso regularizations and ridge regression. However, they have some shortcomings, such as the fact that they could be more effective when the dimensionality is substantially high, and the number of instances is limited. Similar to this, our regularization approach has several drawbacks, which are listed below 1) Neither feature selection nor feature reduction are permitted; 2) Choosing an appropriate value for λ is challenging since it is a continuous number, and selecting a single suitable value by trying a million times would be computationally expensive and time-consuming.

10. Conclusion. The primary goal of this study is to lessen the load of extensive annotation needed for precise image categorization in this field. Additionally, the study demonstrates a method to enhance the effectiveness of a limited number of annotations without relying solely on deep learning models. It is essential to highlight that the proposed active learning model can be integrated with several machine learning approaches, including deep and non-deep learning models. To optimize the efficiency of our research for this assignment, we employed a methodology known as ts-CNN. According to experimental findings, using a sizable collection of BC histopathology images using a confidence-boosting technique leads to a considerable reduction in annotation costs compared to a random selection. Furthermore, when paired with a slicing technique that boosts confidence, the deep learning framework outperforms existing approaches in terms of performance, accuracy with 98.2 %, and annotation costs. Thus, by employing this strategy, the costs of annotating medical applications can be significantly decreased, and the applications' capacity to react to real-world medical conditions can be improved.

REFERENCES

[1] Sung, H. et al.. "Global cancer statistics 2020: Globocan estimates of incidence and mortality worldwide for 36 cancers in 185 countries". CA Cancer J. Clin. 71, 209–249 (2021).

[2] Feng, Y. et al. Breast cancer development and progression: Risk factors, cancer stem cells, signalling pathways, genomics, and molecular pathogenesis. Genes Dis. 5, 77–106 (2018).

[3] Elfgen, C. et al., Comparative analysis of confocal microscopy on fresh breast core needle biopsies and conventional histology. Diagnostics. Pathol. 14, 1–8 (2019).

[4] Hameed, Z.et.al. A. Breast cancer histopathology image classification using an ensemble of deep learning models. Sensors 20, 4373 (2020).

[5] Aresta, G. et al. Bach: Grand challenge on breast cancer histology images. Med. Image Anal. 56, 122–139 (2019).

[6] Jiang, Y.et.al. Breast cancer histopathological image classification using convolutional neural networks with small se-resnet module. PLoS ONE 14, e0214587 (2019).

[7] Sharma, S.et.ali,.A potential feature extractor in breast cancer histology images classification. ICT Express 8, 101–108 (2022).

[8] Yan, R. et al.Breast cancer histopathological image classification using a hybrid deep neural network. Methods 173, 52–60 (2020).

[9] Bianconi.et.al. Experimental assessment of colour deconvolution and colour normalization for automated classification of histology images stained with hematoxylin and eosin. Cancers 12, 3337 (2020).

[10] Salvi, M.et.al. Te impact of pre-and post-image processing techniques on deep learning frameworks: A comprehensive review for digital pathology image analysis. Comput. Biol. Med. 128, 104129 (2021)

[11] Roy, S.et.al. A study about colour normalization methods for histopathology images. Micron 114, 42–61 (2018).

[12] Zhu, C. et al. Breast cancer histopathology image classification through assembling multiple compact cnns. BMC Med. Inform. Decis. Mak. 19, 1–17 (2019).

[13] Zambonelli, et al. Accurate, reliable and active histopathological image classification framework with Bayesian deep learning. Sci. Rep. 9, 1–12 (2019).

[14] Hao, Y. et al. Breast cancer histopathological image classification based on deep semantic features and grey level co-occurrence matrix. PLoS ONE 17, e0267955 (2022)..

[15] Guo, S.-W. Zhang.et.al."Network control principles for identifying personalized driver genes in cancer," Briefings in Bioinformatics, 2019.

[16] Xu, Z.et.al. "Large scale tissue histopathology image classification, segmentation, and visualization via deep convolutional activation features," BMC bioinformatics, vol. 18, p. 281, 2017.

[17] Henriksen, J. F.et.al. "The efficacy of using computer-aided detection (CAD) for detection of breast cancer in mammography screening: a systematic review," Acta Radiol., vol. 60, no. 1, pp. 13-18, Jan. 2019.

[18] Tang, A.et.al. "CapSurv: Capsule Network for Survival Analysis With Whole Slide Pathological Images," IEEE Access, vol. 7, pp. 26022-26030, 2019.

[19] Yang et al.,. "Cascade of multi-scale convolutional neural networks for bone suppression of chest radiographs in gradient domain," Med. Image Anal., vol. 35, pp. 421-433, 2017.

[20] Milletari, N.et.al. "V-Net: Fully Convolutional Neural Networks for Volumetric Medical Image Segmentation," in Proc. Fourth International Conference on 3d Vision, 2016, pp. 565-571.
[21] BenTaieb, H.et.al. "A structured latent model for ovarian carcinoma subtyping from histopathology slides," Med. Image Anal., vol. 39, pp. 194-205, Jul. 2017.
[22] Goceri, B.et.al. "Quantitative validation of anti-PTBP1 antibody for diagnostic neuropathology use: Image analysis approach," Int. J. Numer. Meth. Biomed., vol. 33, no. 11, Nov. 2017
[23] Hou, A.et.al. "Unsupervised histopathology image synthesis," arXiv preprint arXiv:1712.05021, 2017.
[24] Jia, X.et.al. "Constrained Deep Weak Supervision for Histopathology Image Segmentation," IEEE Trans. Med. Imaging, vol. 36, no. 11, pp. 2376-2388, Nov. 2017.
[25] Ocampo et al., "Classification and Mutation Prediction from Non-Small Cell Lung Cancer Histopathology Images Using Deep Learning," J. Thorac. Oncol., vol. 13, no. 10, pp. S562-S562, Oct. 2018.
[26] Goceri. "Diagnosis of Alzheimer's disease with Sobolev gradient-based optimization and 3D convolutional neural network," Int. J. Numer. Meth. Biomed., vol. 35, no. 7, p. e3225, Jul. 2019.
[27] Shaban, C.et.al. Stain Style Transfer for Digital Histological Images," in Proc. 16th IEEE Int. Symp. Biomed. Imaging, 2019, pp. 953-956.
[28] Mateusz Buda. A systematic study of the class imbalance problem in convolutional neural networks, Neural Networks, 2018, 106, pp.249-259.

Edited by: Anil Kumar Budati
Special issue on: Soft Computing and Artificial Intelligence for Wire/Wireless Human-Machine Interface
Received: Nov 9, 2023
Accepted: Jan 6, 2024